Journal of Membrane Science 423–424 (2012) 362–370

Contents lists available at SciVerse ScienceDirect

Journal of Membrane Science

journal homepage: www.elsevier.com/locate/memsci

Fabrication of polyethersulfone-mesoporous silica nanocomposite ultrafiltration membranes with antifouling properties

Jian Huang [a], Kaisong Zhang [a,*], Kun Wang [b], Zongli Xie [c], Bradley Ladewig [b], Huanting Wang [b,*]

[a] Institute of Urban Environment, Chinese Academy of Sciences, No. 1799, Jimei Road, Xiamen 361021, China
[b] Department of Chemical Engineering, Monash University, Clayton, VIC 3800, Australia
[c] CSIRO Materials Science and Engineering, Private Bag 33, Clayton South, VIC 3169, Australia

ARTICLE INFO

Article history:
Received 29 May 2012
Received in revised form
24 July 2012
Accepted 20 August 2012
Available online 27 August 2012

Keywords:
Nanocomposite membrane
Mesoporous silica
Antifouling
Irreversible fouling

ABSTRACT

Fouling is regarded as the bottleneck in membrane filtration process. One of the practical strategies to decrease fouling is the use of advanced anti-biofouling membrane material. In this study, mesoporous silica (MS) particles was synthesized as inorganic fillers, and fabricated with polyethersulfone (PES) to achieve nanocomposite membranes with antifouling properties by phase inversion method. The effect of the MS particles on the microstructure and properties of the resulting hybrid membranes were investigated by scanning electron microscopy (SEM), thermal gravitational analysis (TGA), and ultrafiltration (UF) experiments. The results indicated that the nanocomposite membrane with 2% MS exhibited excellent hydrophilicity, water permeability and good antifouling performance. In addition, the TGA results showed that the introduction of the MS particles improved the thermal stability of the nanocomposite membranes. The protein adsorption on the membrane surface decreased significantly from 45.8 μg/cm^2 to 21.4 μg/cm^2 when the MS content increased from 0% to 2%. Most importantly, the protein UF experiments revealed that the incorporation of MS particles reduced membrane fouling, especially irreversible fouling, which reduced dramatically. No benefit was gained from higher MS content (4%), which resulted in significant particle agglomeration.

1. Introduction

Ultrafiltration technology has found wide application for concentration, purification and fractionation of various products in many fields such as the food, medical and biotechnological industries, or as a pre-treatment stage prior to reverse osmosis treatment [1]. However, most commercial ultrafiltration membranes are made from hydrophobic polymers such as polyethersulfone (PES), polysulfone (PS), polypropylene (PP) and polyvinylidene fluoride (PVDF) [2,3], which are susceptible to membrane fouling caused by the deposition of organic pollutants on the membrane surface or adsorption into the membrane pores. Membrane fouling is still a major problem, which impacts the operating costs of UF and restricts its practical application [4]. Membrane fouling includes reversible and irreversible fouling. Reversible fouling can be easily removed by hydraulic cleaning such as backwashing and cross-flushing. However, irreversible fouling can only be overcome by chemical reagents, and repeated chemical cleanings may reduce the membrane performance. Membrane fouling causes a decline in flux and increased energy consumption, while the necessary chemical cleaning procedures add costs and decrease membrane life. Therefore, many investigators tried to find ways to reduce membrane fouling, especially irreversible fouling, to improve the cost effectiveness of UF membranes.

Generally, making membranes more hydrophilic is a common strategy to reduce membrane fouling. Much effort has been devoted to improving hydrophilicity of the conventional hydrophobic membranes by using various techniques, including coating [5,6], grafting hydrophilic species onto the membrane surfaces [7,8], and blending with hydrophilic polymer or inorganic fillers [9,10]. Among these methods, blending with inorganic particles has attracted a great deal of interest due to availability of different types of functional inorganic particles. A variety of inorganic fillers such as titanium dioxide (TiO_2), alumina (Al_2O_3), zirconium (ZrO_2), silica (SiO_2) and Fe_3O_4 have been used to fabricate inorganic–polymer composite membranes [11–16]. Many of these studies indicate that membrane modification enhanced performance, by improving water permeability, mechanical strength, and fouling resistance. However, some researchers report that the non-porous particles tend to migrate to the membrane surface during the phase separation process [14], which leads to a decrease in the effective filtration area of the membrane. Furthermore, the impermeability of the nonporous particles blended into

* Corresponding authors. Tel.: +86 592 6190782.
E-mail addresses: kszhang@iue.ac.cn (K. Zhang), Huanting.Wang@monash.edu (H. Wang).

0376-7388/$ - see front matter © 2012 Elsevier B.V. All rights reserved.
http://dx.doi.org/10.1016/j.memsci.2012.08.029

the polymer matrix does not directly contribute to the enhancement of the membrane transport properties, so the improvement in membrane permeability has been quite limited.

Mesoporous silica (MS) has been studied extensively for various applications due to its high surface areas, narrow pore size distributions and adjustable mesopore sizes [17,18]. MS has been found to increase the permeability of mixed matrix membranes without sacrificing their selectivity due to its good compatibility with the polymer matrix, and it has been widely used to fabricate nanocomposite gas separation membranes to enhance both gas permeability and selectivity [19–21]. For instance, mesoporous silica sphere-polysulfone mixed matrix membranes were prepared for the separation of H_2/CH_4 and CO_2/N_2 mixtures. The thermal stability and mechanical performance of the membranes were enhanced by the incorporation of the particles and H_2/CH_4 separation performance was optimized by blending 8 wt% MS into the polymer [22]. However, no-one has investigated the utilization of mesoporous silica for the preparation of mixed matrix ultrafiltration membranes.

PES is one of the most common ultrafiltration membrane materials due to its outstanding mechanical strength, excellent thermal and chemical stability [7–11]. In the present study, ordered mesoporous silica was synthesized and was used to fabricate MS–PES nanocomposite membranes. The main advantage of our research is related to the use of silica with an ordered mesoporous structure. The application of mesoporous particles should improve the filler-polymer compatibility and enhance the particle dispersion in the matrix. In addition, the porous nature of the fillers gives them a high affinity to water, which should enhance the water content of the membrane and facilitate water transport through the membrane. Furthermore, the functional –OH group on the mesoporous silica should improve the hydrophilicity of the membrane and have adverse effect on the fouling resistance of the membrane. The aim of this study was to fabricate and characterize PES–MS mixed matrix membranes and to determine the optimum loading of inorganic filler to produce an enhancement in terms of permeability and antifouling properties. A series of experiments, such as SEM, water contact angle (CA) and TGA, were carried out for membrane characterization. The mechanism of membrane antifouling performance improvement caused by incorporation of MS was studied and an optimal loading of MS was proposed.

2. Experimental

2.1. Materials

PES (E6020P, BASF Co., Germany) was dried at 110 °C in an oven overnight prior to use in the casting solution preparation. *N*,*N*-dimethylformamide (DMF), poly ethylene glycol (PEG, M_w=400), cetyltrimethylammonium bromide (CTAB),tetraethylorthosilicate (TEOS), absolute ethanol, bovine serum albumin (BSA) and hydrochloric acid (36–38%) were obtained from Sigma Aldrich. Other regents were all of analytical grade and used without further purification. The water used in all experiments was distilled water. BSA solution (1 g/L, pH 7.0) was prepared using 0.2 M phosphate buffer solution.

2.2. Synthesis of mesoporous silica

The synthesis of mesoporous silica followed a similar process to that reported by Cai et al. [23]. Typically, 2.1 mL of sodium hydroxide aqueous solution (2 M) was mixed with 288 mL distilled water. Then, 0.6 g of CTAB was added and the mixture was heated at 80 °C while stirring until a clear solution was obtained. To this clear solution, 3 mL of TEOS was added dropwise with vigorous stirring. The reaction mixture was then stirred at 80 °C for 2 h. The product was centrifuged, washed with excess distilled water and then dried at ambient temperature. Finally, to extract CTAB from the MS, the synthesized product was refluxed in a solution of 150 mL ethanol and 2 mL hydrochloric acid (36–38%) at 78 °C for 12 h, centrifuged, washed with the distilled water, and then dried in an oven at 50 °C. The extraction process was repeated several times to completely remove the template (CTAB), and the prepared MS particles were obtained in powder form.

2.3. Preparation of MS/PES composite membrane

Different amounts (0%, 1%, 2% and 4% based on the solution weight) of dry mesoporous silica particles were added into DMF, the solution was ultrasonicated for 30 min to ensure good dispersion of the particles. 10% of PEG-400 and 18% of PES were then dissolved in the solution while stirring for 24 h at 60 °C until a uniform solution was obtained. The casting solution was then degassed at 60 °C overnight without stirring to completely remove any gas bubbles. The solution was then cast onto a glass plate to produce a flat sheet membrane (200 μm thick) by the phase inversion method. The fabricated membranes were immersed in fresh distilled water to remove all the residual solvent and pore-forming agent before characterization. The resultant membranes were kept in water prior to ultrafiltration experiments. Table 1 shows the compositions of the casting solution.

2.4. Characterization

The nitrogen sorption isotherm was obtained on a Micromeritics ASAP 2020MC instrument at −196 °C. The specific surface area of mesoporous silica was calculated using the multiple-point Brunauer Emmett Teller (BET) method. The pore size distribution was determined from the adsorption branch using the Barrett–Joyner–Halenda (BJH) method. Transmission electron microscopy (TEM) specimens were prepared using a cryostat-microtome (Ultracuts, Reichert Leica), and were picked up by a copper films (200 mesh, ProSciTech).

Morphological structures of the prepared PES membranes were examined using a scanning electron microscope (SEM, JSM-6300F, JEOL). The membrane samples were frozen and fractured in liquid nitrogen, and both the surface and cross section of the samples were gold sputtered for observation. Elemental mapping was conducted with the SEM microscope equipped with energy-dispersive X-ray spectroscopy (EDX).

The hydrophilicity of the membrane was determined by measuring the contact angle of the membrane surface with a contact angle goniometer (CAM200, KSV Instruments Ltd). At least five water contact angles at different locations on the membrane surface were recorded to get a reliable value.

The membrane porosity ε (%) was defined as the volume of the pores divided by the total volume of the porous membrane. The porosity of the different membranes was calculated using Eq. (1) [24].

$$\rho(\%) = \frac{(W_w - W_d)/D_w}{(W_w - W_d)/D_w + (W_d/D_p)} \times 100\% \quad (1)$$

Table 1
PES nanocomposite membranes with different MS contents.

No.	PES (wt%)	PEG-400 (wt%)	DMF (wt%)	MS* (wt%)
M0	18	10	72	0
M1	18	10	71	1
M2	18	10	70	2
M3	18	10	68	4

* The percentage of MS is based on the total amount of casting solution.

where ρ is the porosity of membrane (%), W_w is the wet sample weight (g), W_d is the dry sample weight (g), D_w (0.998 g/cm^3) and D_p(0.37 g/cm^3) is the density of the water and polymer, respectively. Three samples for each membrane were measured and the averaged value was reported.

Mean pore radius r_m (μm) was determined by the filtration velocity method. According to Guerout–Elford–Ferry equation, r_m was calculated as follows [25]:

$$r_m = \sqrt{\frac{(2.9-1.75\varepsilon) \times 8\eta l Q}{\varepsilon \times A \times \Delta P}} \quad (2)$$

where η is the water viscosity (8.9×10^{-4} Pa s), l is the membrane thickness (m), Q is the volume of the permeate water per unit time (m^3 s^{-1}), A is the effective area of the membrane (m^2) and ΔP is the transmembrane pressure (Pa).

The FTIR spectra of the membranes were recorded with a FTIR-ATR spectrometer (Perkin-Elmer) in the wavenumber range of 3500–500 cm^{-1}. The thermal behavior of the membranes was determined using a thermogravimetric analyzer (TGA, Perkin Elmer) over a temperature range of 25–800 °C at a heating rate of 5 °C/min under oxygen atmosphere.

2.5. Water uptake, pure water permeability and solution rejection

Water uptake tests were conducted to evaluate the adsorption of water to membranes with mesoporous silica. Pieces of different membrane samples were immersed in deionized water at room temperature for 24 h and the weight of wetted membrane (W_w) was measured after mopping it with a filter paper. The dry weight (W_d) was determined after 24 h drying at 60 °C, the water uptake ratio was calculated by the following [26]:

$$U = \left(\frac{W_w - W_d}{W_d}\right) \times 100\% \quad (3)$$

A Sterlitech HP4750 stirred cell filtration system was used to evaluate the filtration performance of membranes. The effective area of the membrane was 12.6 cm^2. All the experiments were performed at room temperature (21 ± 1 °C). To measure the pure water permeation, each membrane was initially compacted for 1 h at 400 kPa to get a steady flux, and then the flux (J_{W1}) was recorded at 200 kPa every 5 min until a steady flux was obtained. Molecular weight cut-off (MWCO) of the membrane was determined using the proteins with different molecular weight such as tripsin (20 kDa), pepsin (35 kDa), egg albumin (45 kDa) and BSA (69 kDa) [14]. The protein solutions were prepared by dissolving it in phosphate buffer saline (PBS) solution (1 g/L, pH 7.0). The rejection of proteins (R) was calculated by the following equation:

$$R = 1 - \left(\frac{C_p}{C_f}\right) \times 100 \quad (4)$$

where C_p and C_f is the permeate concentration and the feed concentration, respectively. Proteins concentrations of both feed and permeate solutions were measured by a UV–vis spectrophotometer (Spectra Max M2, Molecular) at 280 nm. It should be noted that the permeate solution was collected at the first 5 min for the rejection study and all of the filtration processes were repeated three times and the average data was reported. The smallest molecular weight that is rejected by 90% is taken as the MWCO of the membranes [27].

2.6. Analysis of membrane fouling

After water flux tests, pure water was changed to 1 g/L BSA solution in PBS (pH=7.0) and the permeate flux (J_p) profile with time was recorded every 5 min to determine the dynamic fouling resistance of the membrane. After 60 min of protein filtration, the membrane was cleaned with distilled water under magnetic stirring for 30 min, and then the pure water was introduced to repeat the flux measurement (J_{w2}).Three samples were performed for each experiment and the average value was reported.

In order to evaluate the fouling-resistance of the membranes, the flux recovery ratio (FRR) was calculated by using the following equation:

$$FRR = \left(\frac{J_{w_2}}{J_{w_1}}\right) \times 100\% \quad (5)$$

The flux loss caused by reversible (R_r) and irreversible (R_{ir}) protein fouling in the filtration were defined by:

$$R_r = \left(\frac{J_{w_2} - J_p}{J_{w_1}}\right) \times 100\% \quad (6)$$

$$R_{ir} = \left(\frac{J_{w_1} - J_{w_2}}{J_{w_1}}\right) \times 100\% \quad (7)$$

The membrane fouling was composed of reversible and irreversible fouling, so the degree of flux loss caused by total protein fouling (R_t) in the ultrafiltration was defined as:

$$R_t = R_r + R_{ir} = \left(\frac{J_{w_1} - J_p}{J_{w_1}}\right) \times 100\% \quad (8)$$

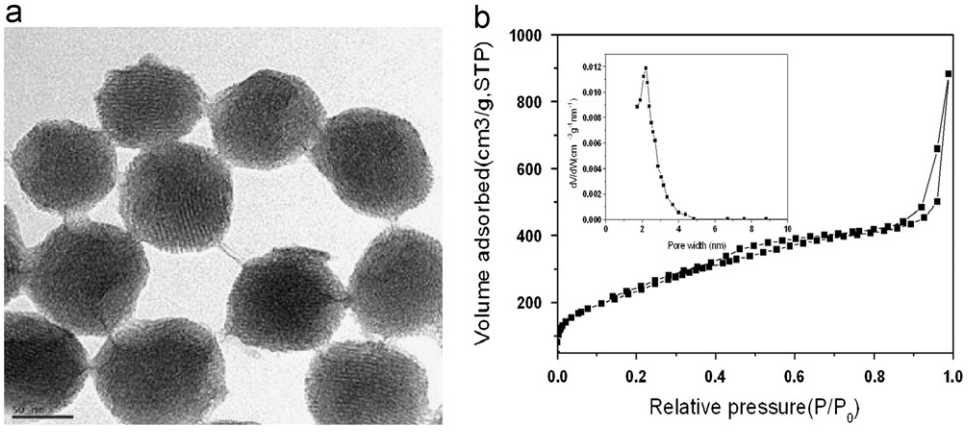

Fig. 1. TEM (a), nitrogen sorption isotherm of mesoporous silica (b). The inset is the corresponding BJH pore distribution.

For static adsorption-fouling experiment, a piece of membrane (3×3 cm) was immersed into a solution of BSA/PBS (1 g/L, pH=7.4), which was placed in a vial filled with 10 mL of protein solution. These vials were then incubated at a water bath of 25 °C for 12 h to reach equilibrium. The amount of protein adsorbed on membrane was calculated by comparing the absorption intensity variation at 280 nm recorded by a UV–vis spectrometer. All data were averaged from three samples taken from the same membrane.

3. Results and discussion

3.1. Characterization of mesoporous silica particles

The TEM image (Fig. 1a) shows that the prepared silica fillers are monodisperse spherical nanoparticles with a particle size of ca. 100 nm, and there are relatively ordered mesopore channels in the particle. The nitrogen adsorption/desorption isotherms and pore size distribution of the mesoporous silica are shown in Fig. 1b. An increase in nitrogen uptake at a relative pressure of $0.4 < P/P_0 < 0.6$ occurs due to the capillary condensation inside the mesopores, the nitrogen adsorption at above $P/P_0=0.9$ should arise from capillary condensation of N_2 in interparticle voids. The specific surface area for MS is 868.9 m^2/g, calculated by using the Brunauer–Emmett–Teller (BET) method. As shown in Fig. 1b, the particles exhibit a narrow pore size distribution, peaking at 2.2 nm. These results indicate mesoporous silica nanoparticles have been successfully prepared for use as inorganic fillers in the preparation of the composite membranes.

3.2. Characterization of prepared membranes

3.2.1. Morphologies of membranes

The membrane surface and cross-section morphologies were observed by SEM. Fig. 2 shows that the pure PES membrane and the MS/PES membranes exhibit similar surface morphology. Comparing with base PES membrane (M0), some aggregates of MS nanoparticles were embedded on the surface of MS/PES hybrid membrane. During the phase separation process, the hydrophilic MS particles would migrate from PES matrix toward water bath so as to reduce interfacial energy between the casting solution and the water bath. As the MS loading in the casting solution increased, more particles can be observed on the membrane surface. The Si mapping on the surface of membrane M2 is also shown in Fig. 2. It can be seen that elemental Si (the red spots) is evenly distributed on the membrane surface. Fig. 3 shows that all the membranes exhibit the typical asymmetric structure, consisting of a skin layer as a selective layer and a thick finger-like sub-layer and sponge like bottom layer. For the pure PES membrane, it can be seen that the macrovoids and finger-like pores were separated by the spongy-like structure, and a clear boundary between sub-layer and bottom layer can be observed. However, the macrovoids and finger-like pores were almost joined for the membrane with 1% MS loading (M1), and no boundary between sub-layer and bottom layer can be observed.

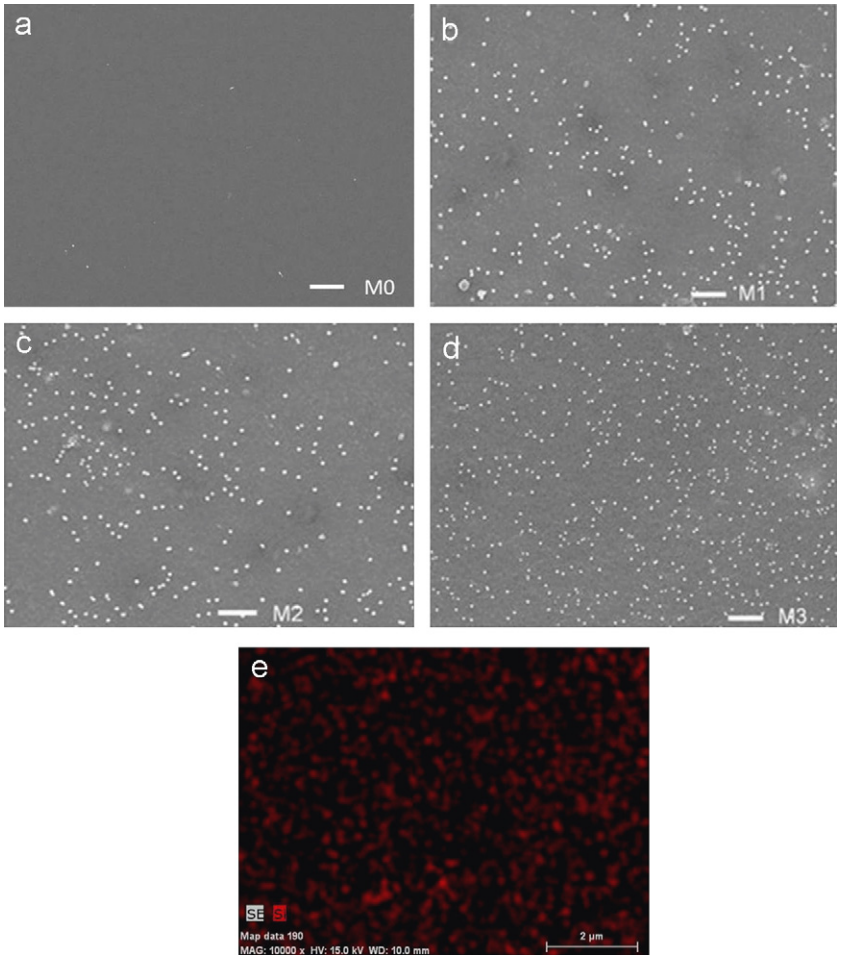

Fig. 2. Surface SEM images of M0, M1, M2 and M3 (scale bar is 10 µm), Energy-dispersive X-ray (EDX) Si mapping on the surface of MS–PES membrane (M2). (For interpretation of the references to color in this figure legend, the reader is referred to the web version of this article.)

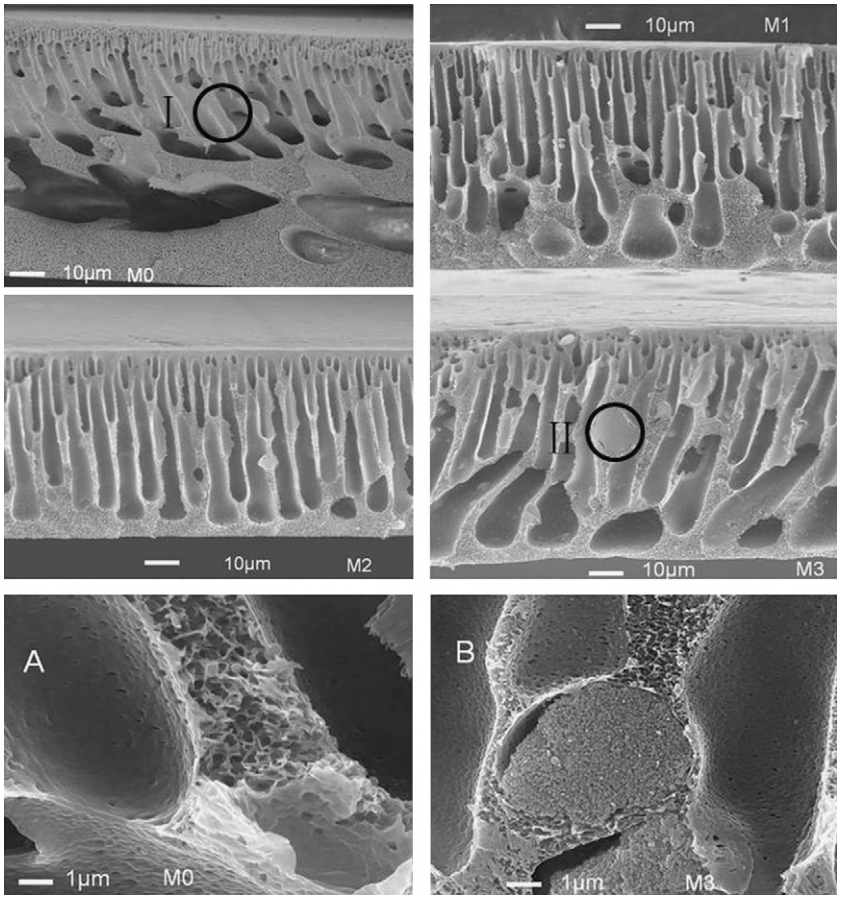

Fig. 3. Cross sectional SEM images of the PES ultrafiltration membranes with different loadings of MS particle (M0, M1, M2 and M3). (A) magnification of section I in M0, (B) magnification of section II in M3.

When the MS loading increased to 2%, an evident improvement in the membrane structure could be viewed from the SEM images (Fig. 3, M2), the finger-like microvoids enlarged across the membrane thickness, and become wider close to the back side of membrane. A similar trend could also be noted for M3, but not as evident as that of M2. This result may be explained by the delayed exchange rate of solvent and nonsolvent in the phase inversion process due to the increased viscosity of the PES–MS blend solution, the formation of macrovoids in the membrane is suppressed. In addition, it should be noted that an excessive loading of MS could result in agglomeration and pore blocking as can be observed in Fig. 3B. During the phase inversion process, nuclei of the polymer-poor phase formed due to the exchange of the solvent and nonsolvent. As the nuclei of the polymer-poor phase had more water than the surrounding blended solution, hydrophilic MS particles would migrate from the blended solution to the nuclei of the polymer-poor phase. When the blended solution solidified, MS aggregated and stayed in some nuclei, which caused the formation of membrane structure shown in Fig. 3(B). However, no obvious MS agglomeration was observed in M1 and M2, the reason maybe that the prepared MS has pore diameter of about 2 nm, the polymer chains are able to penetrate into the mesopores of the filler to form a homogenous casting solution, which would improve the dispersion of MS in the membrane.

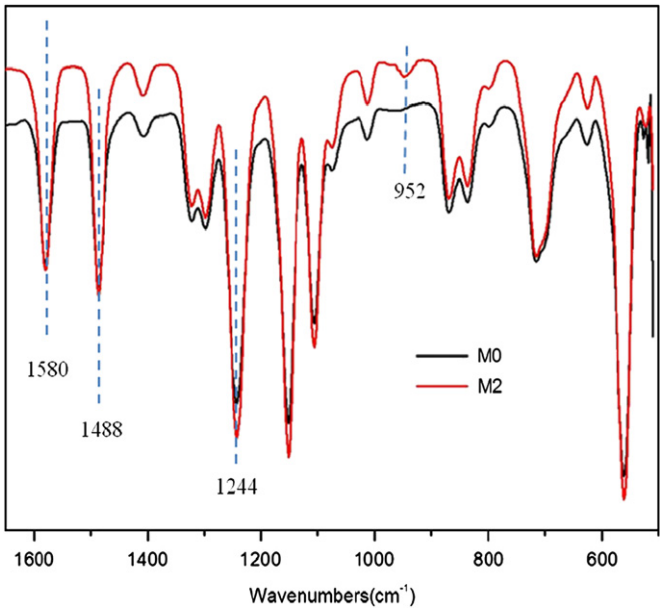

Fig. 4. FTIR spectra of pure PES (M0) membrane and PES–MS nanocomposite membrane (M2).

3.2.2. *Surface chemistry of membranes*

Fig. 4 shows the IR spectra of the pure PES membrane (M0) and the MS–PES nanocomposite membrane (M2). For both membranes, the absorption bands, which correspond to the polyethersulfone structure, are observed at 1580 cm^{-1} (benzene ring stretching), 1488 cm^{-1} (C–C bond stretching) and 1244 cm^{-1} (aromatic ether stretching), respectively [28]. Furthermore, a new peak at 952 cm^{-1} appears for the membrane prepared with addition of mesoporous

Table 2
Contact angle, porosity and pore size of PES–MS membranes with different mesoporous silica.

Membrane no.	MS content (wt%)	CA (°)	Porosity ε (%)	Pore size r_m (μm)	MWCO (kDa)
M0	0	68.1	69.2	0.0129	45
M1	1	61.8	74.8	0.0137	45
M2	2	56.6	75.9	0.0146	45
M3	4	57.1	74.9	0.0128	45

silica, which is ascribed to the Si–OH stretching [29]. The IR spectra data indicate that the MS particles were incorporated in the membrane successfully and the –OH group formed on the membrane surface which could enhance the membrane hydrophilicity.

3.2.3. Hydrophilicity, porosity, pore size and MWCO of membranes

To evaluate the surface hydrophilicity of the prepared membranes with different amounts of mesoporous silica, surface contact angles of membranes were measured, and the results are presented in Table 2. As shown in this table, the contact angle of the PES membrane decreases as the incorporation of the MS particles increases, which indicates the hydrophilicity of membrane is improved. As confirmed by the FTIR spectra, a large amount of –OH on the MS–PES nanocomposite membrane should be responsible for the hydrophilicity improvement. However, increasing the MS amount to more than 2% does not further improve membrane hydrophilicity. Zhang et al. also reported the similar results [30].The possible reason was that the aggregation of the MS particles occurred on the membrane surface when the MS content was further increased to 4% in the membrane. Overall, the membrane with 2% MS (M2) had the best hydrophilicity due to the well dispersed hydrophilic mesoporous silica in the membrane, which is expected to result in high antifouling performance of the membrane.

The modified membranes also show higher porosity than that of the pure PES membrane, and M2 has the highest porosity among the PES–MS nanocomposite membranes. The reason could be the increase in the pore size and the pore number due to the addition of the MS particles, as observed from the cross section images of the membranes. The addition of the MS particles does not have any significant effect on the surface pore size of the membrane and all the membranes have a MWCO of 45 kDa.

3.2.4. Thermal stability of the membranes

The thermal stability of PES membrane was evaluated by TG analysis. Fig. 5 shows the TGA results of pure PES and the composite membranes with different loadings of mesoporous silica. The small mass loss between 25–400 °C for all the membranes is due to the loss of the adsorbed water and/or the residual DMF solvent (its boiling point is 153 °C) within the membranes. The major mass loss occurs in the temperature range of 400–750 °C corresponding to the polymer combustion. Interestingly, it can be observed that with the incorporation of the MS particles, the degradation temperature of the membrane increases, as indicated by the shift of the TG curves. The introduction of the MS particles improved the thermal stability of the membranes, and which is expected for the inorganic-polymer nanocomposite membranes [31,32]. Previous research attributed this phenomenon to the fact that the fillers improve mass transport barrier effects to both the oxidizing atmosphere and the volatile compounds generated during degradation [33].

The residual masses after TG analysis are 4.1%, 8.3% and 13.0% for M1, M2 and M3, respectively. Considering the complete combustion of the pure polyethersulfone, the increase in the residual mass should correspond to the amount of MS added. This confirms the successful incorporation of the MS particles in the membranes.

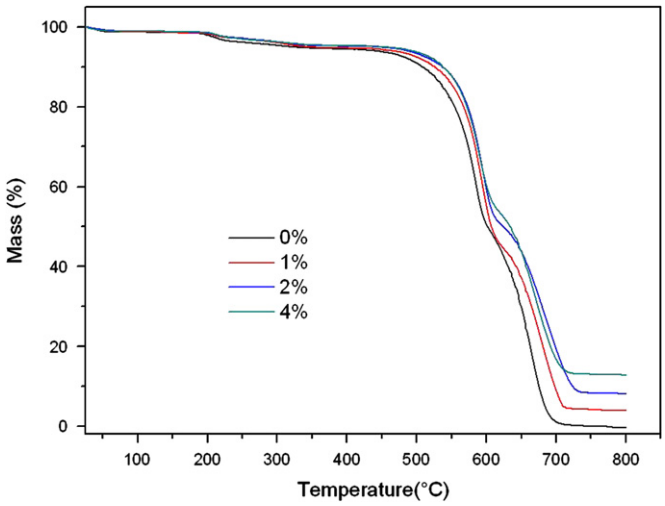

Fig. 5. TGA curves for M0, M1, M2 and M3.

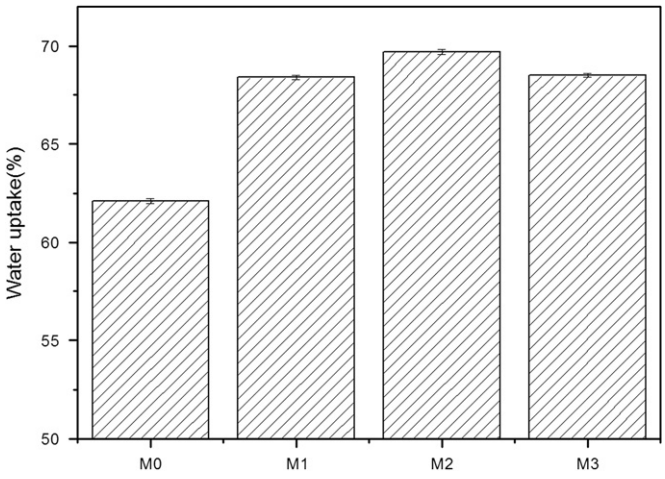

Fig. 6. Water uptake of PES membranes with different MS loadings.

3.2.5. Pure water uptake and ultrafiltration performance

Incorporation of MS particles to PES membrane can change the water uptake of membranes. As shown in Fig. 6, the water uptake capacity first increased with increasing the MS loading, and then decreased when the MS amount reached 4%. The incorporation of the MS particles enhanced the hydrophilicity of the membrane, and resulted in an increase in water uptake. The subsequent decrease in water uptake for M3 could be due to the agglomeration of MS in the membrane.

Ultrafiltration experiments were conducted to study the permeability of PES membranes with different contents of MS particle. Fig. 7 shows the time-dependent fluxes of pure water and BSA solution for the membranes. All the modified membranes exhibited higher pure water flux than that of pure PES membrane and M2 has the highest value of 180.2 L/m^2 h. The water flux of M3 is lower than those of M1 and M2. Considering the pure PES membrane and PES–MS membranes have similar surface pore size and MWCO, the increase in water flux with the introduction of MS can be explained as follows. Firstly, the hydrophilicity of the membranes increased as the MS particles was incorporated.

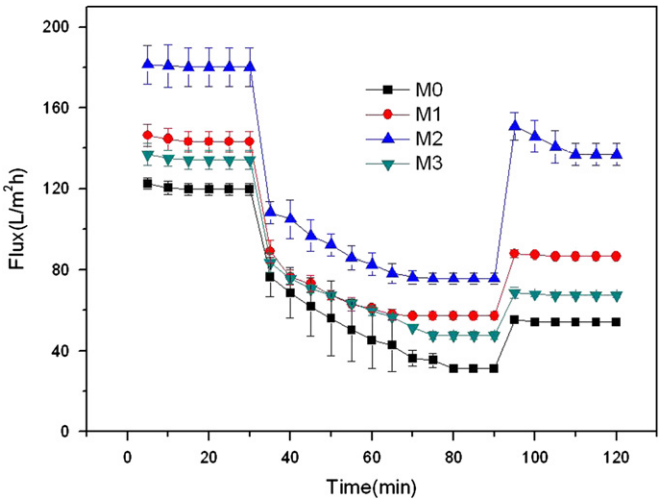

Fig. 7. Time-dependent flux during filtration of 1 g/L BSA solution at 0.2 MPa for M0, M1, M2 and M3.The ultrafiltration process includes four steps: pure water flux measurement, BSA solution ultrafiltration, water washing, and pure water flux measurement of the cleaned membranes.

The pure PES membrane was hydrophobic but the PES membrane became more hydrophilic with incorporation of the MS particles, which improved the water uptake and permeation. Secondly, the incorporation of the MS, enlarged the finger-like pore size of the membrane, and improved the inter-connectivity throughout the membrane thickness, which, decreased the membrane hydraulic resistance and increased water flux. However, with further increasing MS loading to 4%, water flux decreased, which might be attributed to the agglomeration of MS particles in the membrane.

In Fig. 7, the measured fluxes of protein solution were lower than that of pure water and dropped dramatically in the first 30 min before stabilizing. Some protein molecules in the feed can deposit on the membrane surface, this deposition causes an abrupt drop in flux at early stage of the test. At the same time, some protein molecules can be swept from the membrane surface under stirred conditions. A relatively steady flux (J_p) was obtained at the end of test because of the equilibrium achieved between the deposition and sweeping [34]. The protein solution flux (J_p) for the pure PES membrane is 31.2 L/m^2 h. With the incorporation of the MS, the protein fluxes increased substantially to 57.3 L/m^2 h and 75.8 L/m^2 h for M1 and M2, respectively, and then decreases to 47.7 L/m^2 h when the MS content rose to 4%. The BSA rejection ratio was 96.0% for pure PES membrane, and 96.8%, 96.1% and 97.2% for M1, M2 and M3, respectively. The incorporation of MS has little influence on the rejection performance of the membranes, which was expected because of the similar pore sizes of the membranes.

3.3. Antifouling performance of the membranes

After 60 min of BSA ultrafiltration, the water fluxes of the cleaned membrane were measured again. FRR values were calculated and presented in Fig. 8. The fouling resistance of a membrane was usually evaluated by the value of R_{ir} or FRR. Higher values of FRR reflected lower persistent protein adsorption to the membrane operated during the ultrafiltration process [35]. The FRR value is only 45.2% for the base PES membrane, meaning the serious membrane fouling occurring on the base membrane surface. FRR increased to the highest value of 76.2% as the MS loading increased to 2%, and then decreased to 50.3% with a 4% MS content in the membrane. The reason is that the pure PES membrane is less hydrophilic than the PES–MS membranes, the protein molecules can absorb on the membrane surface easily,

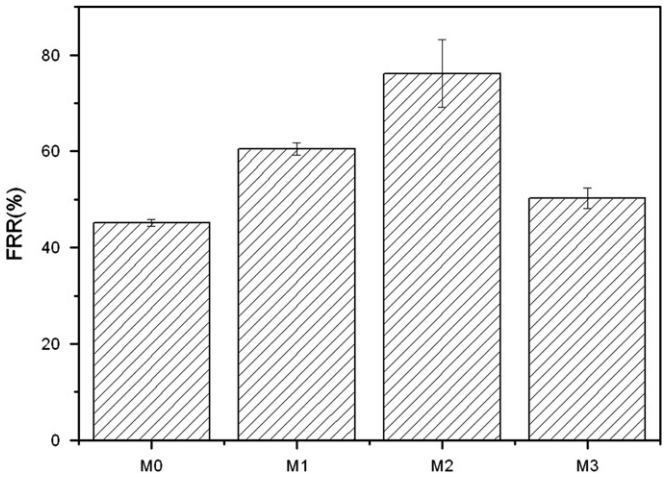

Fig. 8. Flux recovery ratio (FRR) for M0, M1, M2 and M3.

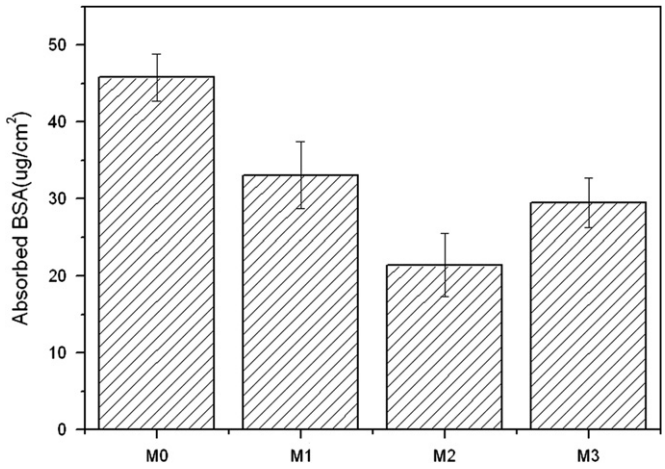

Fig. 9. BSA adsorption amount for M0, M1, M2 and M3.

and they cannot be removed by simple water washing. The incorporation of the MS particles improved the membrane hydrophilicity, resulting in the enhancement of the antifouling performance. The FRR value decreased when the MS content increased to 4% due to the pore blockage as can be seen in Fig. 2. The trapped protein in the membrane pores cannot be washed out easily, so that the M3 has lower flux recovery. All the FRR values of modified PES membranes are higher than that of base PES membrane, meaning that the modification of PES membranes with mesoporous silica additive does improve the fouling resistance.

The effect of MS particles on membrane antifouling performance was also investigated through the BSA static adsorptive fouling test. Fig. 9 shows that the MS–PES membranes exhibit more resistance protein adsorption and M2 shows the lowest BSA adsorption amount. In fact, the pure PES membrane adsorbed around 2.1 times greater than that of M2. It is well known that hydrophilic surfaces have better anti-fouling properties for organic protein materials including BSA [36]. In our case, the incorporation of the MS improved the membrane surface hydrophilicity and decreased BSA adsorption.

To study the fouling properties of the prepared PES membranes in more detail, the total membrane fouling, the reversible and irreversible membrane fouling were calculated. A summary of R_t, R_r and R_{ir} values of PES membranes is given in Fig. 10. It can be seen that M2 has not only a highest R_r value, but also a lowest R_{ir} value. The well dispersed MS particles in M2 improved the antifouling performance of the membrane due to the enhancement of the

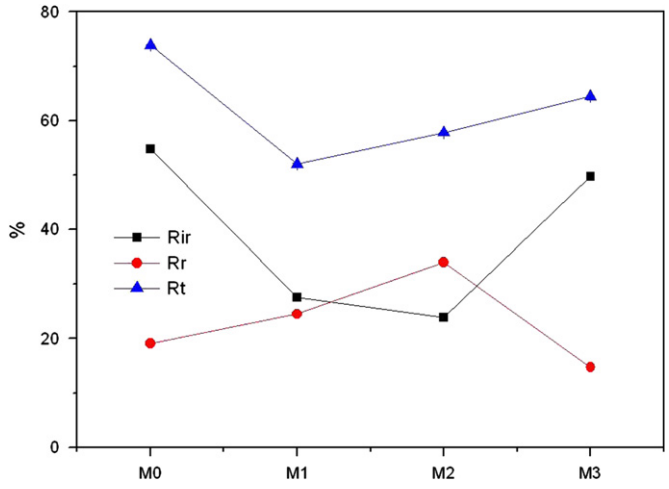

Fig. 10. Summary of the total fouling ratio (R_t), reversible fouling ratio (R_r), and irreversible ratio (R_{ir}) for M0, M1, M2and M3.

hydrophilicity which was supported by the results of the contact angle tests. These results indicate that M2 has the best antifouling properties which are in good agreement with the FRR results.

4. Conclusion

Mesoporous silica modified PES membranes were fabricated by the phase inversion method. The hydrophilic and porous nature of the mesoporous silica had a strong impact on membrane performance. The SEM results indicated that the addition of the mesoporous silica enlarged the pore size in the sub-layer and improved the interconnectivity of pores between the sub-layer and bottom layer. The membrane hydrophilicity, porosity, water uptake and thermal stability were increased due to the introduction of the hydrophilic mesoporous silica. Filtration performance results suggested that the modified membranes had higher pure water permeation than that of pure PES membrane. The pure water flux of the membrane with 2% mesoporous silica reached 180.2 L/m^2 h with a BSA rejection of 96.1%. Further increasing the particle content decreased the membrane flux due to the agglomeration of the particles. Antifouling performance results showed that the modified membrane exhibited better antifouling property, and the M2 membrane had the best fouling resistance for both static and dynamic BSA fouling experiments.

Acknowledgments

The authors thank the Knowledge Innovation Program of CAS (No. KZCX2-YW-452) and the Program for Key International S&T Cooperation Projects, MOST (2009DFB90120),Australia Research council for financial support. Jian Huang is grateful to the China Scholorship Council (CSC) for a SCS scholarship. Huanting Wang thanks the Australia Research Council for a Future Fellowship. The authors are also grateful to the reviewers, Robert Field and Micheal Semmens for their helpful comments.

References

[1] K.J. Howe, M.M. Clark, Fouling of microfiltration and ultrafiltration membranes by nature waters, Environ. Sci. Technol. 36 (2002) 3571–3576.
[2] M.S. Araki, C.M. Coutinho, L.A.G. Gon, L.A. Viotto, Solvent permeability in commercial ultrafiltration polymeric membranes and evaluation of the structural and chemical stability towards hexane, Sep. Purif. Technol. 71 (2010) 13–21.
[3] J. Lindau, A.S. Jönsson, Adsorptive fouling of modified and unmodified commercial polymeric ultrafiltration membranes, J. Membr. Sci. 160 (1999) 65–76.
[4] J. Mansouri, S. Harrisson, V. Chen, Strategies for controlling biofouling in membrane filtration systems: challenges and opportunities, J. Mater. Chem. 20 (2010) 4567–4586.
[5] A. Razmjou, J. Mansouri, V. Chen, M. Lim, R. Amal, Tatiana nanocomposite polyethersulfone ultrafiltration membranes fabricated using a low temperature hydrothermal coating process, J. Membr. Sci. 380 (2011) 98–113.
[6] Y.H. La, B.D. McCloskey, R. Sooriyakumaran, A. Vora, B. Freeman, M. Nassar, J. Hedrick, A. Nelson, R. Allen, Bifunctional hydrogel coatings for water purification membranes: improved fouling resistance and antimicrobial activity, J. Membr. Sci. 372 (2011) 285–291.
[7] P.S. Yune, J.E. Kilduff, G. Belfort, Fouling-resistant properties of a surface-modified poly(ether sulfone) ultrafiltration membrane grafted with poly(ethylene glycol)-amidebinary monomers, J. Membr. Sci. 377 (2011) 159–166.
[8] A. Rahimpour, UV photo-grafting of hydrophilic monomers onto the surface of nano-porous PES membranes for improving surface properties, Desalination 265 (2011) 93–101.
[9] A. Razmjou, J. Mansouri, V. Chen, M. Lim, R. Amal, Titania nanocomposite polyethersulfone ultrafiltration membranes fabricated using a low temperature hydrothermal coating process, J. Membr. Sci. 380 (2012) 98–113.
[10] W.F. Zhao, J.Y. Huang, B.H. Fang, S.Q. Nie, N. Yi, B.H. Su, H.F. Li, C.S. Zhao, Modification of polyethersulfone membrane by blending semi-interpenetrating network polymeric nanoparticles, J. Membr. Sci. 369 (2011) 258–266.
[11] Y.A. Yang, H.X. Zhang, P. Wang, Q.Z. Zheng, J. Li, The influence of nano-sized TiO_2 fillers on the morphologies and properties of PSF UF membrane, J. Membr. Sci. 288 (2007) 231–238.
[12] S. Liang, K. Xiao, Y.H. Mo, X. Huang, A novel ZnO nanoparticle blended polyvinylidene fluoride membrane for anti-irreversible fouling, J. Membr. Sci. 394 (2012) 184–192.
[13] R.A. Zoppi, C.G.A. Soares, Hybrids of Poly(ethylene oxide-*b*-amide-6) and ZrO_2 Sol–gel: preparation, characterization, and application in processes of membranes separation, Adv. Polym. Tech. 21 (2002) 2–16.
[14] G. Arthanareeswaran, T.K.S. Devi, M. Raajenthiren, Effect of silica particles on cellulose acetate blend ultrafiltration membranes: Part I, Sep. Purif. Tech. 64 (2008) 38–47.
[15] Z.Q. Huang, Z.Y. Chen, X.P. Guo, Z. Zhang, C.L. Guo, Structures and separation properties of PAN-Fe_3O_4 ultrafiltration membranes prepared under an orthogonal magnetic field, Ind. Eng. Chem. Res. 45 (2006) 7905–7912.
[16] P. Jian, H. Yanhui, W. Yang, L. Linlin, Preparation of polysulfone-Fe_3O_4 composite ultrafiltration membrane and its behavior in magnetic field, J. Membr. Sci. 284 (2006) 9–16.
[17] C.C. Liu, X.M. Wang, S. Lee, Lisa D. Pfefferle, G.L. Haller, Surfactant chain length effect on the hexagonal-to-cubic phase transition in mesoporous silica synthesis, Microporous Mesoporous Mater. 147 (2012) 242–251.
[18] H.H. Dai, J.T. Yang, J.P. Ma, F. Chen, Z.D. Fei, M.Q. Zhong, A green process for the synthesis of controllable mesoporous silica materials, Microporous Mesoporous Mater. 147 (2012) 281–285.
[19] B. Zornoza, C. Téllez, J. Coronas, Mixed matrix membranes comprising glassypolymers and dispersed mesoporous silica spheres for gas separation, J. Membr. Sci. 368 (2011) 100–109.
[20] K.S. Jang, H.J. Kim, J.R. Johnson, W. Kim, W.J. Koros, C.W. Jones, S. Nair, Modified mesoporous silica gas separation membranes on polymeric hollow fibers, Chem. Mater. 23 (2011) 3025–3028.
[21] S. Kim, E. Marand, Polysulfone and mesoporous molecular sieve MCM-48 mixed matrix membranes for gas separation, Chem. Mater. 18 (2006) 1149–1155.
[22] B. Zornoza, S. Irusta, C. Tellez, J. Coronas, Mesoporous silica sphere-polysulfone mixed matrix membranes for gas separation, Langmuir 25 (2009) 5903–5909.
[23] Q. Cai, Z.S. Luo, W.Q. Pang, Y.W. Fan, X.H. Chen, F.Z. Cui, Dilute solution routes to various controllable morphologies of MCM-41 silica with a basic medium, Chem. Mater. 13 (2001) 258–263.
[24] B. Chakrabarty, A.K. Ghoshal, M.K. Purkait, Effect of molecular weight of PEG on membrane morphology and transport properties, J. Membr. Sci. 309 (2008) 209–221.
[25] C.S. Feng, R. Wang, B.L. Shi, G.M. Li, Y.L. Wu, Factors affecting pore structure and performance of poly (vinylidene fluoride-*co*-hexafluoro propylene) asymmetric porous membrane, J. Membr. Sci. 277 (2006) 55–64.
[26] M. Sivakumar, A.K. Mohansundaram, D. Mohan, K. Balu, R. Rangarajan, Modification of CA: its characterization and application as an UF membranes, J. Appl. Polym. Sci. 67 (1998) 1939–1946.
[27] K.J. Kim, A.G. Fane, R. Ben Aim, M.G. Liu, G. Joansson, I.C. Tessaro, A.P. Broek, D. Bargeman, A comparative study of techniques used for porous membrane characterization: pore characterization, J. Membr. Sci. 87 (1994) 35–46.
[28] H. Susanto, M. Ulbricht, Characteristics, performance and stability of polyethersulfone ultrafiltration membranes prepared by phase separation methodusing different macromolecular additives, J. Memsci. Sci. 327 (2009) 125–135.
[29] L.Y. Yu, Z.L. Xu, H.M. Shen, H. Yang, Preparing and characterization of PVDF–SiO_2 composite hollow fiber UF membrane by sol–gel method, J. Membr. Sci. 337 (2009) 257–265.
[30] Y.Q. Zhang, Z.H. Jin, X. Shan, J. Sunarso, P. Cui, Preparation and characterization of phosphorylated Zr-doped hybrid silica/PSF composite membrane, J. Hazard. Mater. 186 (2011) 390–395.

[31] A.F. Ismail, N.H. Rahima, A. Mustafa, T. Matsuura, B.C. Ng, S. Abdullah, S.A. Hashemifard, Gasseparation performance of polyethersulfone/multi-walled carbon nanotubes mixed matrix membranes, SeP. Purif. Technol. 80 (2011) 20–31.
[32] L.Y. Yu, Z.L. Xu, H.M. Shen, H. Yang, Preparation and characterization of PVDF–SiO_2 composite hollow fiber UF membrane by sol–gel method, J. Membr. Sci. 337 (2009) 257–265.
[33] E. Stanislav, Solovyov, reactivity of gas barrier membranes filled with reactive particulates, J. Phys. Chem. B 110 (2006) 17977–17986.
[34] M.P. Sun, Y.L. Su, C.X. Wu, Z.Y. Jiang, Improved antifouling property of PES ultrafiltration membrane using additive of silica-PVP nanocomposite, Ind. Eng. Chem. Res. 49 (2010) 790–796.
[35] Y. Chang, C.Y. Ko, Y.J. Shiha, D. Quémener, A. Deratani, T.C. Wei, D.M. Wang, J.Y. Lai, Surface grafting control of PEGylated poly(vinylidene fluoride) antifouling membrane via surface-initiated radical graft copolymerization, J. Membr. Sci. 345 (2009) 160–169.
[36] H.Y. Yu, M.X. Hu, Z.K. Xu, J.L. Wang, S.Y. Wang, Surface modification of polypropylene microporous membranes to improve their antifouling property in MBR: NH_3 plasma treatment, Sep. Purif. Technol. 45 (2005) 8–15.